Fuel 304 (2021) 121376

Contents lists available at ScienceDirect

Fuel

journal homepage: www.elsevier.com/locate/fuel

Online dynamic prediction of potassium concentration in biomass fuels through flame spectroscopic analysis and recurrent neural network modelling

Xinli Li [a], Changxing Han [a], Gang Lu [b], Yong Yan [b,*]

[a] School of Control and Computer Engineering, North China Electric Power University, Changping District, Beijing 102206, China
[b] School of Engineering, University of Kent, Canterbury, Kent CT2 7NT, UK

ARTICLE INFO

Keywords:
Biomass
Potassium concentration
Dynamic prediction
Flame spectroscopy
Recurrent neural networks

ABSTRACT

Biomass fuels are widely used as a renewable source for heat and power generation. Alkali metals in a biomass fuel have an significant impact on furnace safety as such metals lead to fouling and slagging in the furnace and corrosion of water pipes. This paper presents a technique for dynamic predicting Potassium (K) concentration in a biomass fuel based on spectroscopic analysis and different recurrent neural networks. A miniature spectrometer is employed to acquire the spectroscopic signals of K in different biomass fuels, including peanut shell, willow, corn cob, corn straw and wheat straw, and their blends. The spectroscopic features of K are extracted. The factors that influence the spectral intensity of K in the biomass fuels are investigated. A basic recurrent neural network (RNN), and its variants, i.e., long short-term memory neural network (LSTM-NN) and deep recurrent neural network (DRNN), are constructed using the spectroscopic signal of K from the spectrometer. The performances of the neural networks for the dynamic prediction of K concentration are compared and analysed theoretically and experimentally. It is found that the relative error in the K concentration prediction through the use of the DRNN model is within 6.34% whilst the LSTM-NN and RNN models give errors slightly greater than this.

1. Introduction

As one of important renewable energy sources, biomass fuels have the advantage of abundant varieties and environmental friendliness [1]. It has been widely used either as a single fuel or a blend of different solid fuels for generating electricity or thermal power. In China, biomass power generation has grown steadily and accounted for about 2% of the total power field from 2006 to 2017, marking that China is the second largest country in the world in the biomass power generation, only after the United State [2]. However, biomass combustion systems often suffer from severe operation problems, including poor combustion stability, low combustion efficiency, and furnace fouling and slagging with potential safety concerns [3,4]. It is known that a biomass fuel contains generally high volatile matter, high fixed carbon concentration, low moisture content and low ash concentration. It also has high alkali metal (Potassium and Sodium) concentrations which are main contributor to furnace fouling and slagging. The potassium concentration is relatively high in the ash and the melting point of the formed compounds is generally low. So, it is molten at a high temperature and easy to slag on the water-cooled wall, reducing the heat conduction efficiency of the boiler [5]. It is therefore highly desirable to detect on-line continuously the fouling and slagging in biomass-fired boilers.

Current techniques available for detecting fouling and slagging in a biomass-fired boiler are mostly off-line, where the samples of ash and slagging are taken, and the ash fusion temperature and alkali metal concentrations are analysed in laboratory. There are some laboratory-based methods which are commonly used off-line to analyse alkali concentration in biomass fuels. They include scanning electron microscopy (SEM), X-ray diffraction (XRD) and X-Ray fluorescence (XRF) [6,7]. Although potassium (K) and sodium (Na) release characteristics during biomass combustion can be obtained, these methods require sophisticated and expensive laboratory equipment and are unsuitable for online operation. As the type of biomass or their blends may change unexpectedly during combustion, there is a pressing need to measure the K concentration online continuously for combustion optimisation under flexible operation conditions.

A burner flame contains extensive information about the fuel and the combustion process. The spectroscopic information of the flame is closely related to flame temperature, fuel properties, operation

* Corresponding author.
E-mail address: y.yan@kent.ac.uk (Y. Yan).

https://doi.org/10.1016/j.fuel.2021.121376
Received 26 March 2021; Received in revised form 28 June 2021; Accepted 1 July 2021
Available online 9 July 2021

Nomenclature

b_c	Bias of the memory unit
b_f	Bias of the forget gate
b_i	Bias of the input gate
b_o	Bias of the output gate
c_t	Memory unit
h_t	Output of the hidden layer
K_u	Kurtosis coefficient
N	Number of samples
S_k	Skewness coefficient
U_c	Weight of hidden layer of the memory unit
U_f	Weight of hidden layer of the forget gate
U_i	Weight of hidden layer of the input gate
U_o	Weight of hidden layer of the output gate
V_f	Weight of output layer of the forget gate
V_i	Weight of output layer of the input gate
V_o	Weight of output layer of the output gate
W_c	Weight of input layer of the memory unit
W_f	Weight of input layer of the forget gate
W_i	Weight of input layer of the input gate
W_o	Weight of input layer of the output gate
$W^{(hh)}$	Weight matrix from h_{t-1} to h_t
$W^{(hx)}$	Weight matrix from x_t to h_t
$W^{(s)}$	Weight matrix from h_t to y_t
x_i	Radiation intensity of the i-th sample
x_t	Input of the input layer
y_t	Output of the output layer
μ	Mean value of the sample
σ	Standard deviation of the sample
$\delta()$	Sigmoid function

conditions, and pollutant emissions. Optical diagnostic techniques, such as laser-induced break down spectroscopy (LIBS), have been used for the online measurement of K and Na concentrations in flames. Hus *et al.* [8] measured the release concentrations of K and Na during the combustion of pine wood pellet based on the LIBS technology, and analysed the peak release concentrations of Na and K during different combustion stages. Liu *et al.* [9] conducted multi-point LIBS measurement on the K release characteristics of poplar wood and corn straw. Flame emission spectroscopy (FES) was also applied to detect alkali release from combustion. Lim *et al.* [10] used optical emission spectroscopy to investigate alkali metal release from biomass combustion. Sadeckas *et al.*[11] measured the emission intensities of Na, Ca, and K from the combustion of single wood and straw pellets doped with known concentrations of Na, Ca, and K by using the ICCD, and analyzed the alkali emission characteristics in terms of relative intensity emission and integrated emission intensity at two different temperatures. With the use of the FES technique and inductively coupled plasma mass spectrometer (ICP-MS), Paulauskas *et al.*[12] studied the capability and the accuracy of chemiluminescence-based sensors to measure the spontaneous emission of K and Na from the combustion of single wood and straw pellets with different alkali concentrations at 1000 °C. The results have shown that the emission intensity of alkali radicals depends on alkali concentrations in the samples and K and Na radical emission intensities increase with alkali concentrations in the samples. He *et al.* [13] established the functional relationship between K concentration and radiation intensity of K characteristic spectral lines in Camphorwood and rice husk flames. For the municipal solid waste incinerators, they developed a portable spectral system to determine temperature and gaseous phase Na and K concentrations. The experimental results have indicated that the released gaseous phase Na and K correlated with both temperature and primary air in incinerators [14]. The functional model between the radiation intensity of Na, temperature, and Na concentration was established based on the FES technique and calibration experiments. Yan *et al.* [15,16] analyzed the characteristics of the temperature and Na concentration in different combustion stages. In the above methods, alkali metal concentration was measured and analyzed off-line under different combustion stages (devolatilization stage, char, and ash stage). At the same time, in order to obtain the concentration of gaseous phase Na and K in the flame, a calibration procedure needs to be followed. However, continuous variations in alkali metal concentration during combustion are seldom considered.

This paper presents the dynamic prediction of K concentration in biomass fuels through flame spectroscopic analysis and recurrent neural network modelling, aiming to achieve continuous monitoring and optimization of combustion processes. The spectroscopic information of the biomass-fired flame is obtained using a miniature spectrometer on a lab-scale combustion test rig under different operation conditions. Three recurrent neural networks, i.e., basic recurrent neural network (RNN), long short-term memory neural network (LSTM-NN) and deep recurrent neural network (DRNN) are constructed based on the spectroscopic features extracted from the spectroscopic information obtained. The RNNs are capable of processing the sequence data of the flame. The nodes between the hidden layers of such networks are connected. The inputs of a hidden layer include not only the output of the input layer but also the output of the previous hidden layer. These unique features enable the RNNs to remember the information of the previous state and apply it to the computation of the current output of the model, making the RNNs to be a potential soft computing approach to predict the K concentration in biomass fuels based on the flame spectroscopic information. A series of experiments were conducted to examine the performance of the RNN models for the dynamic prediction of K concentrations in five typical biomass fuels. Meanwhile, data driven models based on the conventional BP neural network (BP-NN) and support vector machine (SVM) are also established and trained for purpose of a direct comparison with the RNNs. It should be mentioned that, in this study, Sodium (Na), as another common alkali metal in a biomass fuel, is also often regarded as a main contributor for fouling and slagging in biomass combustion. However, the Na concentration in the tested biomass fuels is much lower than the K concentration, and is thus not included in this study.

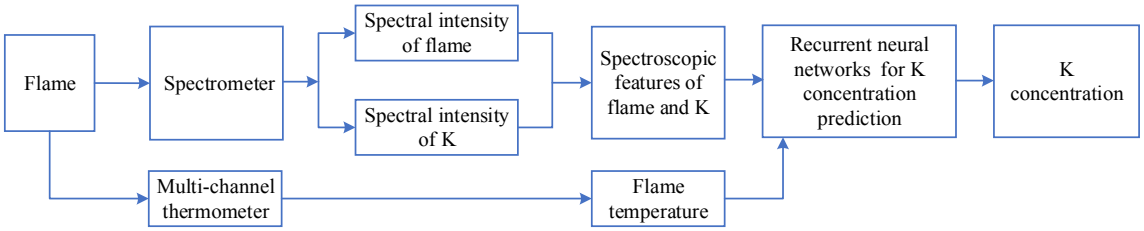

Fig. 1. Block diagram of recurrent neural network models for K concentration prediction.

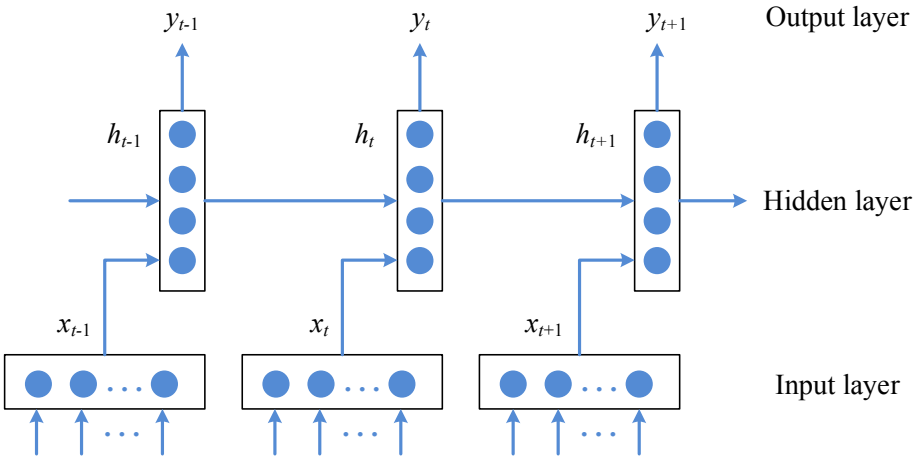

Fig. 2. Architecture of the RNN.

2. Methodology

2.1. Technical strategy

Fig. 1 shows the block diagram of the recurrent neural network models for the dynamic prediction of the K concentration in biomass fuel. The spectroscopic signal of the flame is obtained using a spectrometer over the spectral range from 200 nm to 1100 nm. The spectral intensity of K is also acquired by the spectrometer at the wavelength of 769.89 nm. A set of characteristic parameters, including oscillation frequency, radiant energy, mean, variance, peak-to-peak value, skewness and kurtosis coefficient are then extracted from the signal. These features, together with the flame temperature which is measured by a multi-channel thermometer, are used as the inputs of the prediction models. The expected K concentration (ground truth), which is determined through element analysis, is taken as the output of the models. Three recurrent neural network (RNN) models, including the basic RNN, LSTM-NN and DRNN are trained, validated and tested. It should be noted that the LSTM-NN and DRNN are the variants of the RNN and are also considered for the intended application.

2.2. Recurrent neural network

The RNN is a type of neural network which has a memory function and can be used to process sequential information [17]. The architecture of the RNN is shown in Fig. 2. The RNN has a "memory" which captures information about what has been calculated at the present state. All neurons in the hidden layer are linked in a chain. The output at the current time is not only related to the current input but also depends on the network status in the past. The RNN is widely used in text classification, machine translation, language recognition and image analysis [18,19].

In Fig. 2, x_t and h_t are the input and output of the hidden layer, respectively, and y_t is the output of the output layer at the time t. During the training, the input data is forward-propagated for calculation whilst the error is back-propagated to update weight parameters. The outputs of the hidden layer and the output layer are expressed, respectively, as follows:

$$h_t = f\left(W^{(hh)}h_{t-1} + W^{(hx)}x_t\right) \tag{1}$$

$$y_t = softmax\left(W^{(s)}h_t\right) \tag{2}$$

where $W^{(hh)}$ is the input weight matrix from h_{t-1} to h_t, $W^{(hx)}$ is the input weight matrix from x_t to h_t, $W^{(S)}$ is the weight matrix from h_t to y_t, and f is the activation function [20].

2.3. Long short-term memory neural networks

The LSTM-NN is an improved version of the RNN, which was proposed by Hochreiter and Schmidhuber [21]. The LSTM-NN can effectively process long-distance sequence information and overcome gradient disappearance, gradient explosion and lack of long-term memory ability during the training process of an RNN. Fig. 3 shows the schematic diagram of the LSTM-NN architecture, which is composed of an input gate (i_t), a forget gate (f_t) and an output gate (o_t). The forget gate is a key element, which decides whether to keep the information among neurons during the information transmission. It takes the output of the previous moment and the input of the current moment as inputs, and determines the degree of retention or forgetting through the activation function. The input gate, forget gate and output gate are each connected to a multiplier which controls the input and output of information and the state of each cell.

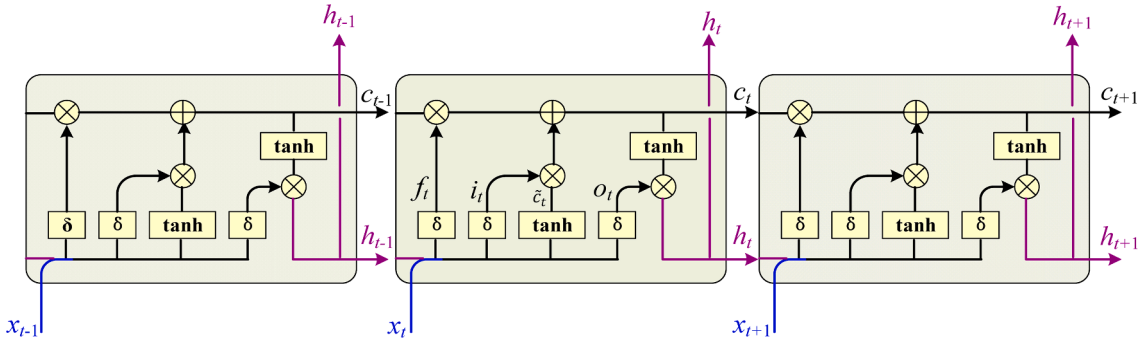

Fig. 3. Architecture of the LSTM-NN.

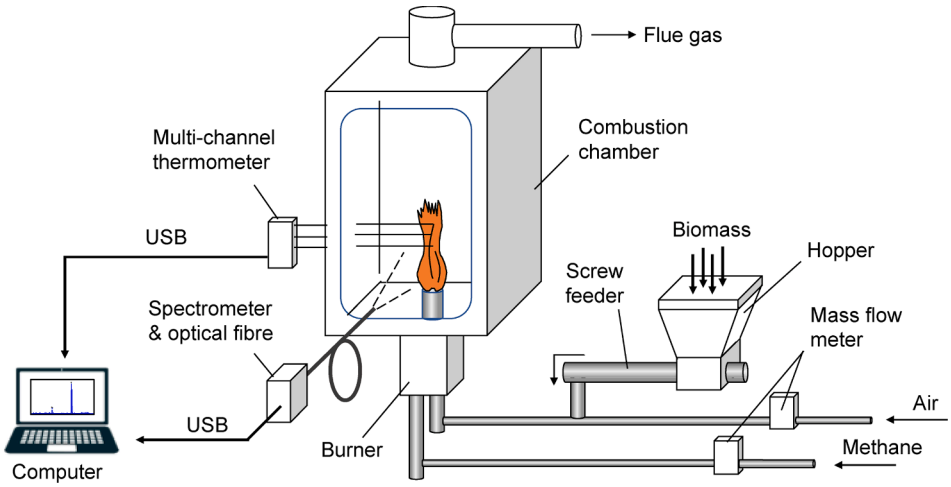

Fig. 4. Experimental setup.

The x_t and h_{t-1}, which present the hidden state of the LSTM-NN at the previous time, are sent to the LSTM-NN through the three gates. For each gate, the input information is calculated using the logic function. The information at the input gate is processed by a nonlinear function, and added with the state of the memory unit, which is processed by the forget gate, to form a new state of the memory unit c_t. Then output h_t of the LSTM-NN cell is formed through the operation of the nonlinear function and the dynamic control of the output gate by using the following equations:

$$f_t = \delta(W_f x_t + U_f h_{t-1} + V_f c_{t-1} + b_f) \quad (3)$$

$$i_t = \delta(W_i x_t + U_i h_{t-1} + V_i c_{t-1} + b_i) \quad (4)$$

$$o_t = \delta(W_o x_t + U_o h_{t-1} + V_o c_t + b_o) \quad (5)$$

$$c_t = f_t c_{t-1} + i_t tanh(W_c x_t + U_c h_{t-1} + b_c) \quad (6)$$

$$h_t = o_t tanh(c_t) \quad (7)$$

where W_f,W_i,W_o,W_c,U_f,U_i,U_o, U_c,V_f,V_i and V_o are the parameters of the matrices, b_f, b_i,b_o and b_c are the bias values, and $\delta()$ is the Sigmoid function.

2.4. Deep recurrent neural network

The DRNN is another improved version of the original RNN. It has more than one hidden layers and can be directly superimposed with multiple hidden layers or directly added one or more fully connected layers between the two hidden layers. The dropout method [22] can be used to prevent overfitting and improve the predictability of the network. For any hidden layer, the neurons are discarded with a certain probability during training, which makes the neurons inactivate randomly. In this way, not all the neurons are trained, and thus, it can avoid the influence of individual neurons on the network. After training, all the neurons will still be used in the calculation [23].

In comparison with the RNN, the DRNN has more network layers and parameters and is able to complete large-scale computing tasks and improve the nonlinear capability of the network. In general, if there is sufficient data, the performance of the DRNN is better than that of the single-layer RNN [24].

3. Results and discussion

3.1. Experimental setup

To examine the effectiveness of the proposed recurrent neural network models for the dynamic prediction of K concentration in biomass fuels, a series of experiments were conducted on a laboratory-scale biomass-air combustion test rig. The experimental setup along with the arrangement of the equipment used is shown in Fig. 4. The test rig consists mainly of a burner resided vertically in an enclosed combustion chamber, a precision screw feeder, and mass flowmeters. A miniature spectrometer (Ocean Optics, USB2000 +) with associated application software was used to acquire the spectroscopic signal of the flame. The spectrometer has an optical fibre probe with an angle of view of 25° and a 2048-pixel linear array CCD, offering good accuracy and repeatability over the considered spectral range (slit: 25 μm, optical resolution: 1.7–2.1 nm at the full width at half maximum, signal-to-noise ratio: 250:1). The height of biomass combustion flame is about 10–15 cm. The distance between the tip of the optical fiber probe and the flame was measured to ensure the tip of the probe optically covers the whole flame. Five typical biomass fuels, i.e., peanut shell, corn cob, corn straw and wheat straw were used in the experiments. The pre-pulverised biomass in the hopper, in the form of powder between 100 and 200 meshes, was fed into the fuel pipe system via the screw feeder and then pneumatically conveyed to the burner before being injected into the combustion reaction zone. The amount of fed biomass is controlled by varying the feeding frequency of the feeder. Methane at a fixed flowrate of 0.5 L/min was used to support the combustion at the initial stage of the biomass-air combustion. A variety of test conditions were then obtained through the combination of different biomass and air supplies. The spectrometer acquired the spectral intensity of the biomass-air flame under different combustion conditions over the spectral range of

Table 1
Proximate and ultimate analysis of the tested biomass fuels (as received).

Biomass	Moisture (%)	Volatile (%)	Ash (%)	Fixed Carbon (%)	C(%)	O(%)	H (%)	S (%)	N (%)
Peanut shell	7.87	70.23	4.21	17.69	43.03	49.52	5.56	0.51	1.37
Willow	9.70	69.93	3.22	17.14	44.67	49.24	5.33	0.56	0.20
Corn cob	5.87	74.55	1.34	18.24	39.68	59.62	<0.1	0.51	0.19
Corn straw	9.50	64.73	9.06	16.70	38.57	44.59	5.17	0.46	1.19
Wheat straw	10.18	58.66	17.58	13.58	32.17	63.18	3.97	0.43	0.26

Table 2
K concentrations of the tested biomass fuels and their blends.

Biomass	Peanut shell	Willow	Willow & Corn cob*	Corn cob	Corn cob & Corn straw*	Corn straw	Corn cob & Wheat straw*	Wheat straw
K concentration(μg/g)	2600	3400	5695	5845	10,943	13,265	16,147	21,495
Measurement uncertainty(μg/g)	±4.93	0.00	±9.93	±19.88	±2.49	±4.99	±2.49	±74.88

Note: * mixed equally (50:50) in mass.

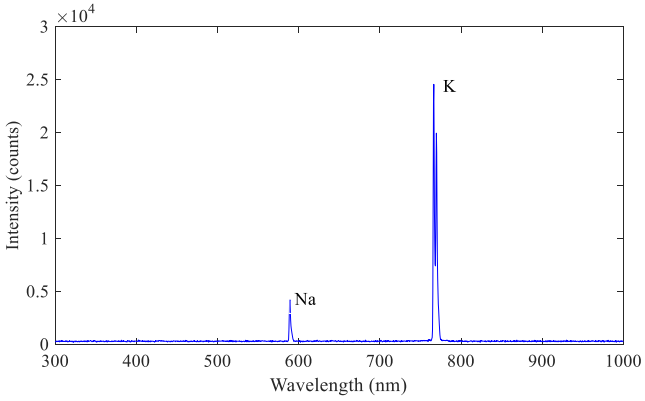

Fig. 5. Spectral intensity distribution of a willow flame.

200 nm −1100 nm. The data acquisition and storage are realized using SpectraSuite software (supplied by the spectrometer supplier). Through this software, the spectral signal of the specified band is acquired with up to three decimal places at most. If the decimal place of the specify band exceeds 1, the spectrometer will automatically locate the signal closest to the specify band. A multi-channel thermometer with 8 k-type thermocouples was also used to measure the temperature of the flame. Both the signals were transmitted to the computer system for further computation.

3.2. Analysis of biomass fuels

The proximate and ultimate analyses of the five biomass fuels are summarised in Table 1. The volatile and fixed carbon are combustible components whereas moisture and ash are non-combustibles. As can be seen, the wheat straw and corn straw have the highest ash content among the five biomass fuels. The K concentration, which has significant influence on slagging, exists in ash. The higher the ash content, the easier the slagging during combustion. The K concentrations of biomass fuels and their blends were analysed with the support of a professional testing agency. Each biomass sample was digested for the element analysis. Each fuel sample had a total of 0.6 g and was split into three equal proportions to conduct three repeated measurements. Each test was done by using firstly nitric acid and hydrofluoric acid to digest the volatile elements of the sample in an enclosed Teflon digestion tank, and then boric acid solution to remove fluoride. The remained solid sample was further digested by a digester (SPEED-WAVE, Germany) to obtain clean solution. Finally, the K concentration in the solution was measured by an inductively coupled plasma atomic emission spectrometer (Leeman Labs Prodigy, USA). Table 2 summarizes the K concentrations of the tested biomass fuels and their blends along with their measurement uncertainties. For each fuel, the K concentration is the mean of the three repeated measurements whilst the measurement uncertainty is the averaged deviation of the three measurements from the mean.

3.3. Spectroscopic characteristics of K in biomass fuels

Fig. 5 shows the spectral intensity distribution of a willow flame, where two peaks at 588.99 nm and 769.89 nm attribute to Na and K elements, respectively. As can be seen, the spectral intensities of Na and K are in the order of 10^4 with a reference to the spectral intensities of the flame in other wavelength ranges.

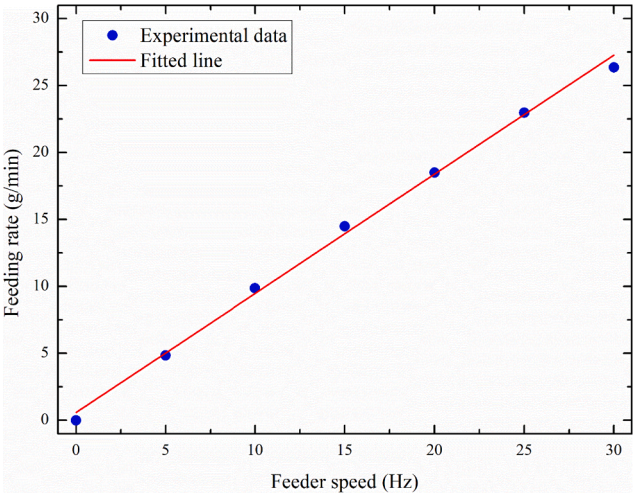

Fig. 6. Screw feeder calibration results.

In order to investigate the spectroscopic characteristics of K in biomass during the combustion process, willow and wheat straw were fired on the test rig. Different fuel flowrates were achieved by alternating the speed of the screw feeder whilst the methane and air flow rates remained constant. The feeding frequency of the screw feeder was set to 3 levels, 2 Hz, 3 Hz and 4 Hz. The miniature spectrometer collected the spectral intensities of the K for the two biomass fuels, which the integration time is 10 ms.

In order to establish the relationship between the amount of fuel and feeding frequency, calibration experiments were conducted. The range of feeding frequency of screw feeder is from 0 Hz to 30 Hz. The amount of fuel was measured at a 5 Hz increment. The calibration test was repeated for 10 times at each speed frequency. The feeding frequency, amount of fuel supplied under different frequency, are plotted in Fig. 6. There exists a linear relationship between the amount of fuel supplied and the feed frequency. Because the diameter of the burner is very small, the burner will be blocked if the fuel feed rate is too high during the test. Therefore, the frequency of the feeder is set to 2 Hz, 3 Hz and 4 Hz in this study. Such feeder rates allow the fuel to be fully injected to the burner for combustion.

The mean spectral intensities and standard deviations (as error bars) of K concentration in willow / wheat straw flames for three different fuel flowrates are plotted in Fig. 7, where each data point was computed for 12,000 readings. It is evident that the spectral intensity of K in the wheat straw flame is higher than that in the willow flame. Table 2 shows that the K concentration in wheat straw is higher than that in willow. This also verified that emission intensity of alkali depends on alkali concentrations in the samples[12]. It is also clear that the spectral intensity of K has positive correlation with the fuel flowrate, i.e., the greater the fuel flowrate, the stronger the spectral intensity of K. The K concentration in the flame increases with the amount of fuel. For a large amount of

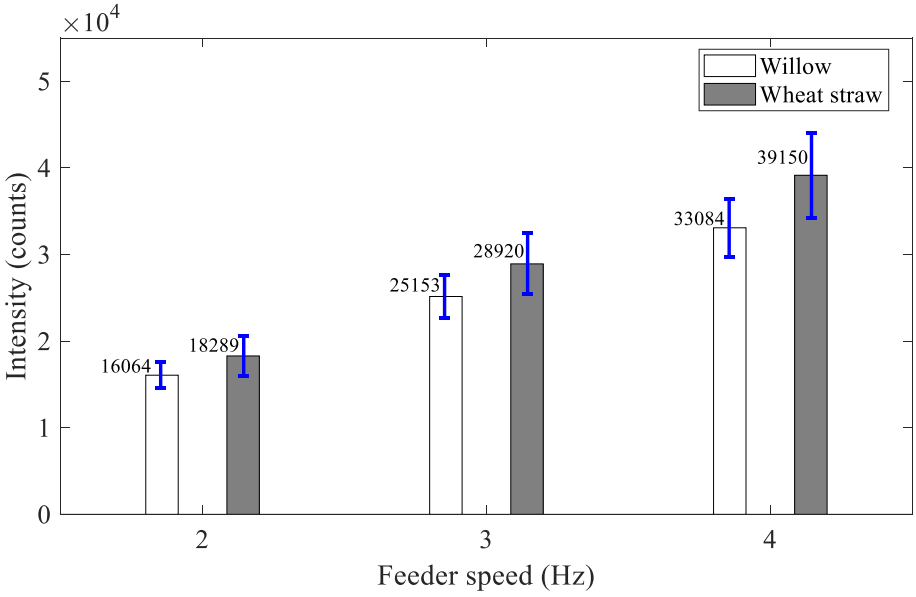

Fig. 7. Mean spectral intensities of K in willow and wheat straw flames under different fuel flowrates.

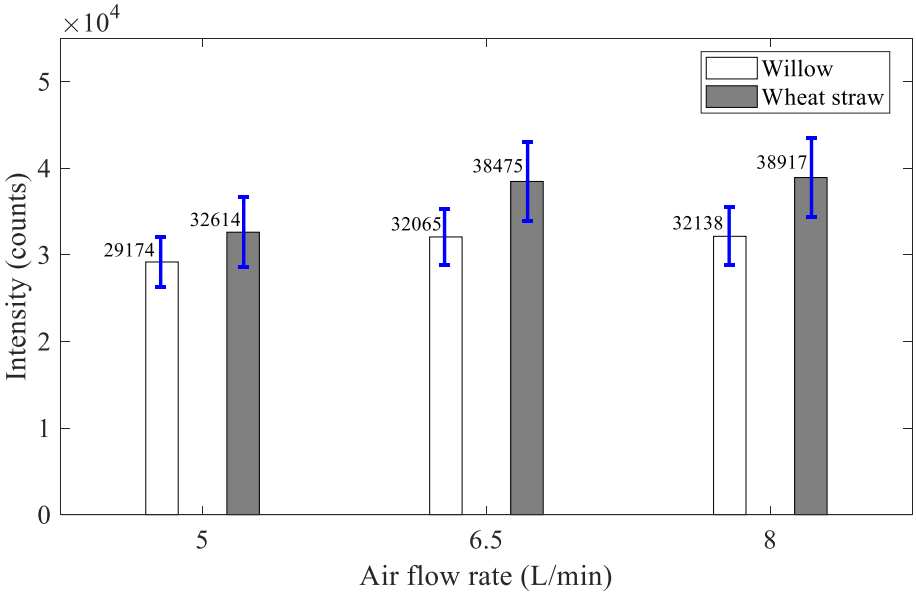

Fig. 8. Mean spectral intensities of K in willow and wheat straw flames under different air flowrates.

fuel, more K concentration is released when the fuel is completely burnt under the same combustion conditions.

Similarly, Fig. 8 illustrates the means and standard deviations (as error bars) of the 12,000 readings in willow / wheat straw flames for three different air flowrates under the feeder speed of 3 Hz and the methane flow rate of 0.5 L/min. As can be seen, the spectral intensity of K in the wheat straw flame is still higher than that in the willow flame. It is related to the K concentration in the fuel. When the amount of fuel is constant, the complete combustion depends on the amount of air. The air flowrate has a little impact on the spectral intensity of K in both the biomass flames. The reason is that it is complete combustion under different air flowrates. It is also found that the spectral intensities of K in the willow / wheat straw flames under air flowrates of 6.5 L/min and 8.0 L/min are about 10% higher than that under 5.0 L/min, which is believed to be due to the increased combustion intensity under higher air flowrates. It illustrates that the spectral intensity of K is related to the biomass fuel type and combustion state.

3.4. Dynamic prediction of K concentration

3.4.1. Data pre-processing and feature extraction

Experimental data for the five biomass fuels and three blends, i.e., willow & corn cob, corn cob & corn straw, and corn cob & wheat straw, mixed equally (50:50) in mass (Table 2), were used to construct the RNN model for the dynamic prediction of the K concentration. Data pre-processing was carried out to remove the dark noise, blackbody radiation and outlier data during the data acquisition. The dark noise was caused by the weak dark current in the CCD sensor of the spectrometer. It was filtered by applying appropriate thresholding values to the spectroscopic signals. The continuous spectrum is excluded in the data pre-processing. It is about 1% of the spectral intensity of K (refer to Fig. 5) in all the cases studied, which is removed by subtracting it from the original signal in the application software.

After the data pre-processing, a total of 12,000 flame spectroscopic data including flame temperature and the corresponding K

Table 3
Flame temperature, oscillation frequency, skewness and kurtosis coefficients of for biomass fuels and their blends.

Biomass	Mean temperature (℃)	Standard deviation of temperature (℃)	Oscillation frequency (Hz)	Skewness coefficient	Kurtosis coefficient
Peanut shells	1024.09	57.05	2.885	−0.006	2.536
Willow	1021.38	43.88	2.912	0.020	2.493
Willow & Corn cob	1000.56	47.92	2.879	0.003	2.452
Corn cob	1051.59	49.39	2.870	0.014	2.430
Corn cob & Corn straw	983.22	55.99	2.953	0.001	2.316
Corn straw	1039.49	49.57	2.937	−0.033	2.393
Corn cob & Wheat straw	970.53	44.59	2.979	−0.027	2.423
Wheat straw	959.43	52.78	3.246	0.019	2.449

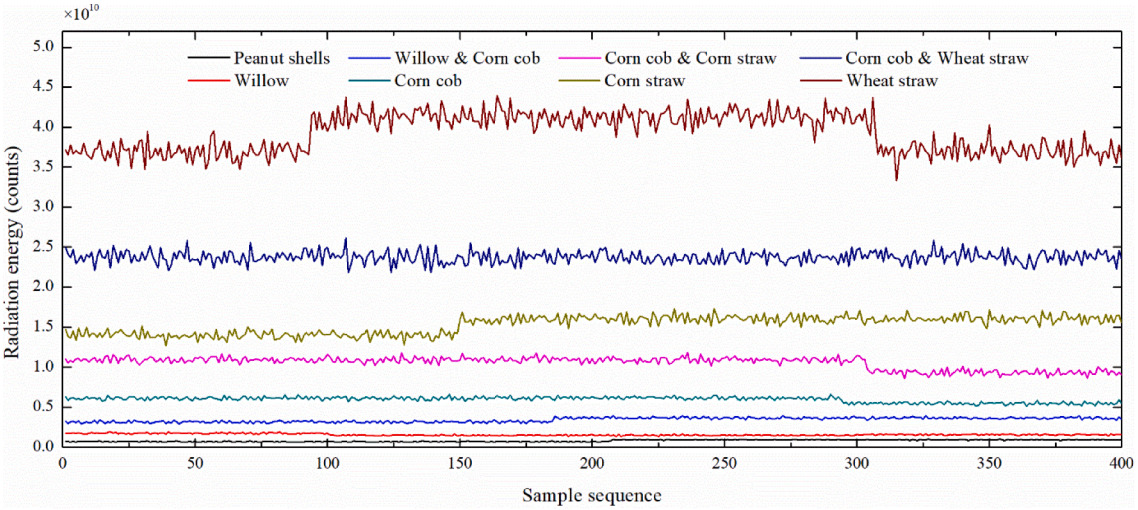

(a) Flame radiation energy.

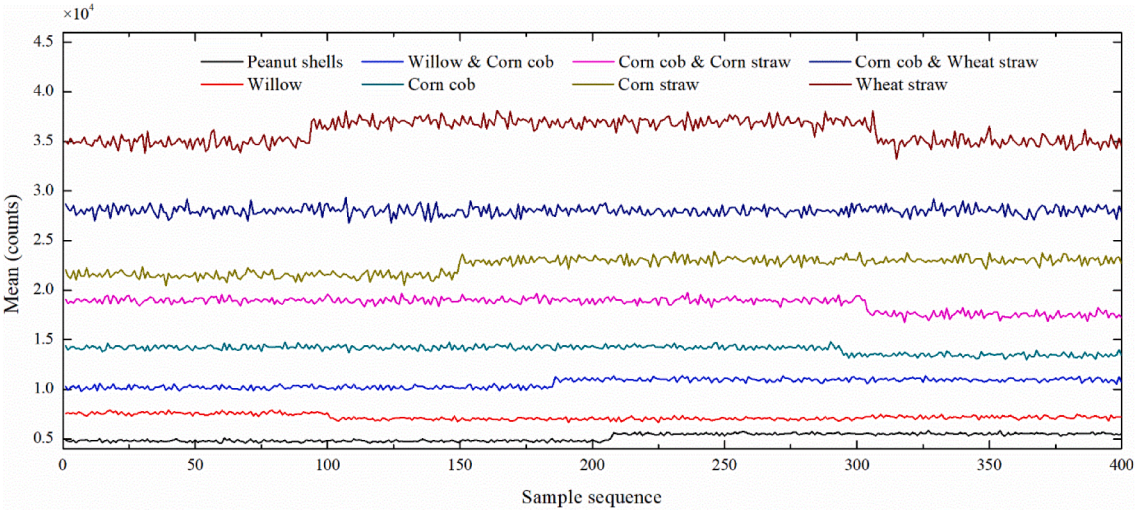

(b) Mean of K spectral intensity.

Fig. 9. Radiation energy, mean, variance and peak-to-peak of K spectral intensity.

concentration (refer to Table 2), were created, where every 30 spectroscopic data were grouped, making a total of 400 sets of sample data for each biomass fuel under each test condition. Five single biomass fuels and three blends (refer to Table 1) were tested at a feeder rate of 3 Hz under the methane flow rate of 0.5 L/min and the air of 5.0 L/min, making a total of 3200 sets of data available for the construction and validation of the three models.

The spectroscopic features of K, including mean, variance, peak-to-peak value, skewness and kurtosis coefficients, were extracted from the spectroscopic signal. The skewness and kurtosis coefficients reflect the asymmetry and steepness of the probability density function of the signal, which are the third- and four-order moments of the signal,

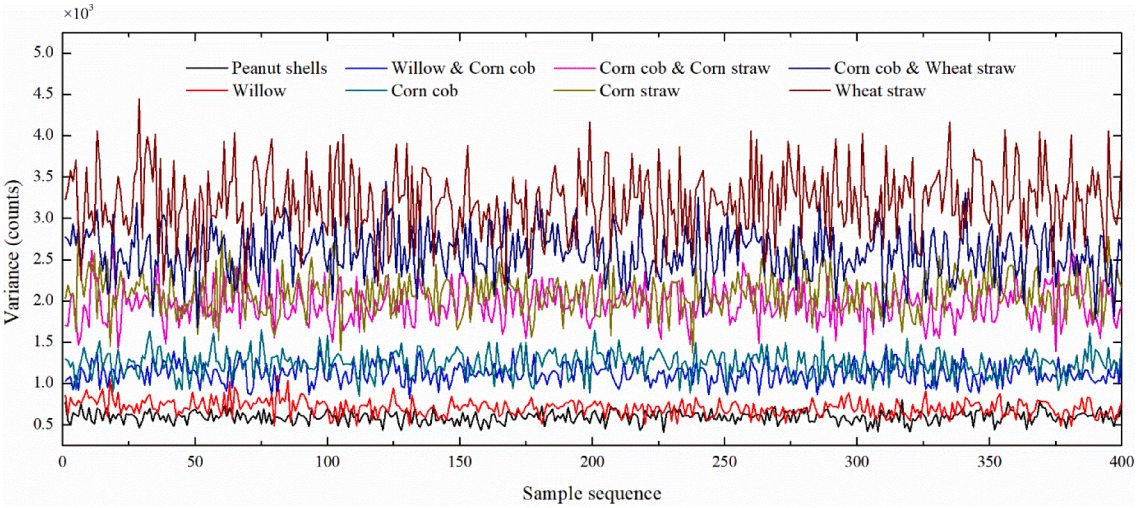

(c) Variance of K spectral intensity.

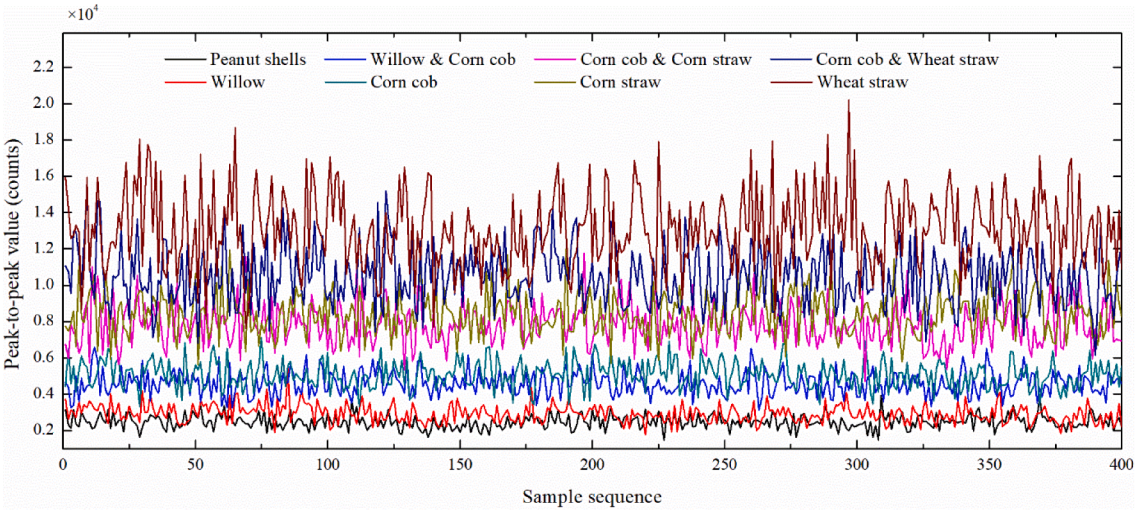

(d) Peak-to-peak value of K spectral intensity.

Fig. 9. (*continued*).

respectively, i.e.,

$$S_k = \frac{1}{N}\sum_{i=1}^{N}\frac{(x_i-\mu)^3}{\sigma^3} \tag{8}$$

$$K_u = \frac{1}{N}\sum_{i=1}^{N}\frac{(x_i-\mu)^4}{\sigma^4} \tag{9}$$

wherex_i is the radiation intensity of the i-th sample of the signal, μ and σ are the mean and standard deviation of the sample, respectively, and N is the number of samples and set to be 30 in this paper.

For each biomass fuel, the mean and standard deviation of flame temperatures, mean oscillation frequency [25] , mean skewness coefficient and mean kurtosis coefficient are summarized in Table 3. A multi-channel thermometer with 8 k-type thermocouples was used to measure the temperatures at different points within the flame region. The thermocouples were arranged in two levels around the flame. For each tested biomass fuel, the flame temperature is the mean of the temperatures given by the 8 k-type thermocouples, which is presented in Table 3. The properties of the biomass, such as moisture, volatile, ash and fixed carbon, all have certain influence on the characteristics of the flame. For instance, the higher the ash content, the lower the thermal efficiency, and hence the relatively lower flame temperature. The volatile and ash content of corn cob is the highest and smallest, respectively, among the five single biomass fuels (refer to Table 1), so the flame temperature of corn cob is higher than that of other biomass fuel. For the five biomass fuels and their blends, the oscillation frequency of the wheat straw flame is slightly higher than that of other fuels and the skewness coefficient of K spectral intensity of the corn straw flame are the highest among the eight biomass fuels.

For each biomass fuel, the flame radiation energy, mean, variance and peak-to-peak value of K spectral intensity are shown in Fig. 9. Fig. 9 (a) and 9(b) indicate that there is a significant difference in the flame radiation energy and mean of K spectral intensity between the biomass fuels. The flame radiation energy and mean of K spectral intensity of wheat straw and corn cob & wheat straw are significantly higher than those of peanut shells and willow. The flame radiation energy and mean of K spectral intensity of the biomass fuels are consistent with the K concentrations. It is noted that small step changes in the radiation energy and mean of K spectral intensity (Fig. 9(a) and 9(b)) exist and this is

Table 4
Structural parameters of the models.

Model	RNN	LSTM-NN	DRNN
Number of hidden layers	1	1	5
Number of neurons in hidden layer	20	20	20 × 5
Number of fully connected layers	6	6	6
Number of fully connected layer neurons	20 × 2, 30 × 2, 10 × 2		
Activation function	tanh, Leaky ReLU		

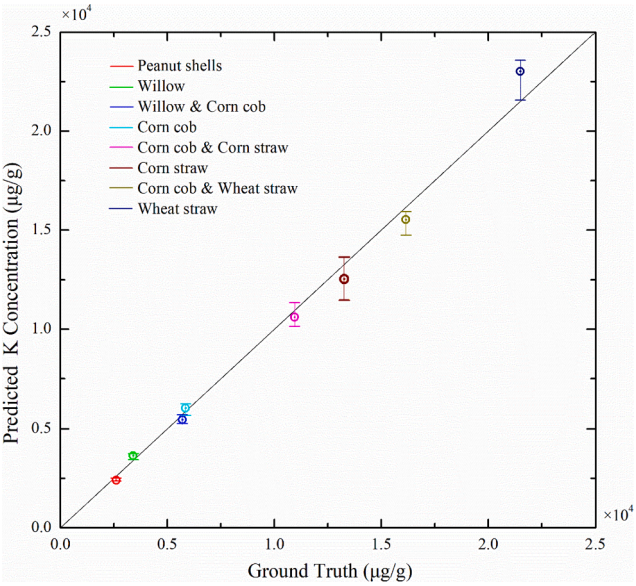

Fig. 10. Predicted K concentration based on RNN with reference to the ground truth.

believed to be related to the type of biomass being fed and the operating characteristics of the screw feeder. The variance and peak-to-peak value of K spectral intensity of the fuels are also very different, as shown in Fig. 9(c) and 9(d). In addition, the variance and peak-to-peak value of the wheat straw and corn cob & wheat straw flames fluctuate widely. The flame radiation energy and oscillation characterise the combustion state of the biomass fuel whilst the flame temperature is related to the K concentration. The characteristic parameters (e.g., mean, variance, peak-to-peak value, skewness and kurtosis coefficients) of the K spectroscopic signal are good descriptors of the K spectroscopic signal and thus can reflect the combustion behaviours of biomass fuels. Therefore, they are selected for the prediction of K content in the models.

3.4.2. *Construction and training of the RNN, LSTM-NN and DRNN models*

Table 4 summarized the network parameters of the three models to be constructed. The inputs to the networks conclude the flame temperature, oscillation frequency, radiation energy and spectroscopic features of K including mean, variance, peak-to-peak value, skewness and kurtosis coefficients. The output of each network is the predicted K concentration. The activation functions of the hidden layer and the fully connected layer are the tanh function and the Leaky ReLU function, respectively. The Leaky ReLU increases the non-linear capability of the network, which makes the networks trained easier and prevents possible neuron inactivation. The key features that are identified to train the models are plotted in Fig. 9. However, since some of the features such as flame temperature, oscillation frequency and skewness and kurtosis coefficients appear very similar between the biomass fuels, only their mean values are listed in Table 3.

3.4.3. *Prediction of K concentration in biomass*

The prediction results of the K concentration using the RNN, LSTM-NN and DRNN models and the corresponding errors are plotted in Figs. 10-13. The *k*-fold cross-validation method was used to evaluate the performance of the models. In this method, the sample data were divided into *k* sets, one of which was selected randomly to test the model, and the rest to train the model. The test set was selected randomly for *k* times, and the accuracy of three prediction models are the average of the prediction accuracies for *k* times. The *k*-fold cross-validation method has an advantage of non-repeated sampling and is often used to optimise the hyper-parameter so that the model has the best generalisation performance. In this study, *k* was selected to be 10, i.e., the 10-fold cross-validation was implemented. A total of 2880 sets of data were used as the training set, and 320 as the test set for 10 times. The final results from the three models for each biomass fuel were the average of 10 readings. The short horizontal bars at each data point in Figs. 10-12 indicate the upper and lower limits of the 10 repeated tests for each biomass fuel. €

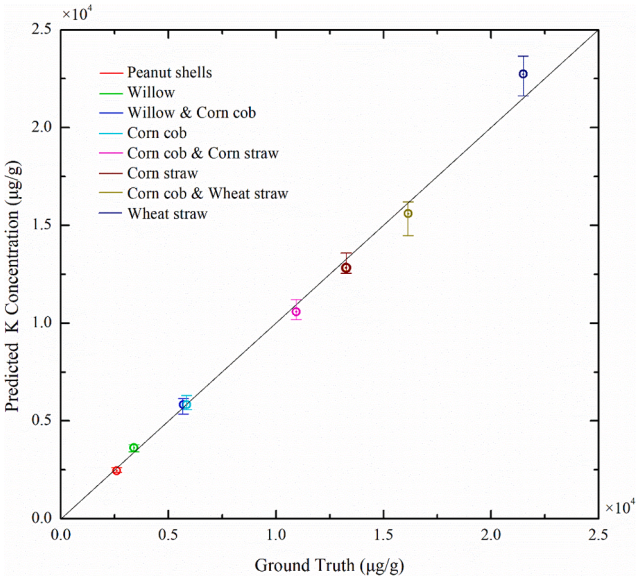

Fig. 11. Predicted K concentration based on LSTM-NN with reference to the ground truth.

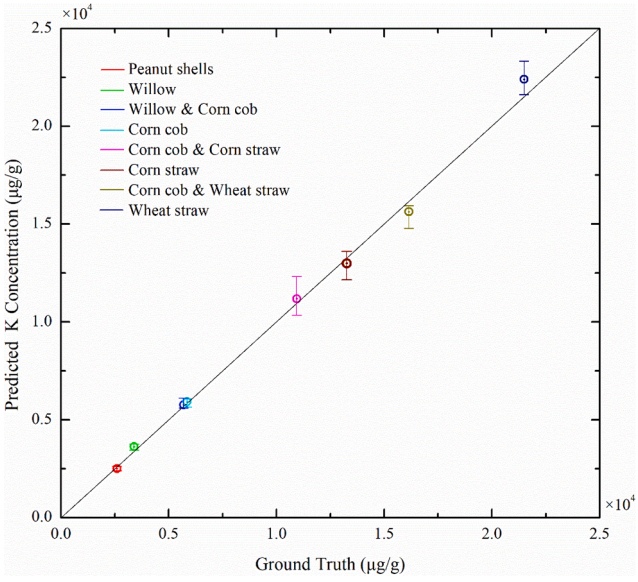

Fig. 12. Predicted K concentration based on DRNN with reference to the ground truth.

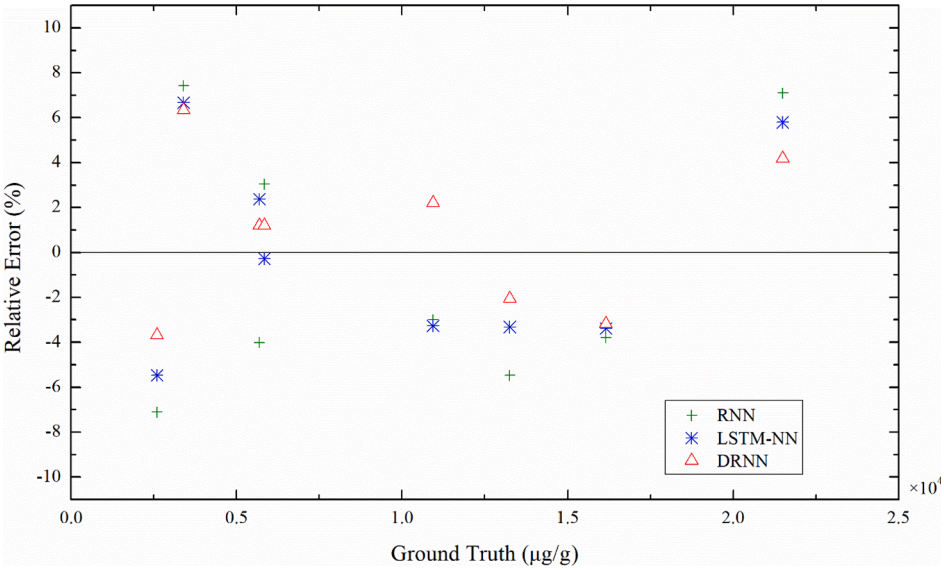

Fig. 13. Relative errors of the three RNN models.

Table 5
Performance comparison of three recurrent neural networks.

	RNN	LSTM-NN	DRNN
RMSE (μg/g)	574.15	563.01	515.29
MAE (μg/g)	481.37	490.99	435.92
MAPE (%)	4.72	4.52	4.04
Maximum errors (%)	7.42	6.67	6.34
Training time (s)	10^{1}	10^{2}	10^{2}
Computational time (s)	10^{-3}	10^{-2}	10^{-2}

Fig. 13 shows that the three RNNs can predict the K concentration in the biomass fuels with a relative error range of (-7.11%, 7.43%), (-5.47%, 6.67%), (-3.18%, 6.34%), respectively, It is clear that the DRNN model yields the smallest error among the three models under all the test conditions. In addition, the relative error for the biomass with higher K concentration (e.g., wheat straw and corn straw) is smaller than that for the biomass with low K concentration (Table 2). This may attribute to a greater signal to noise ratio of the spectral intensity signal under that conditions.

The following metrics are employed to evaluate the prediction performance of the RNN, LSTM-NN and DRNN models.

$$\delta_{\mathrm{MAE}} = \frac{1}{n}\sum_{i=1}^{n}|y_i - y_i^{'}| \tag{10}$$

$$\delta_{\mathrm{MAPE}} = \frac{1}{n}\sum_{i=1}^{n}\left|\frac{y_i - y_i^{'}}{y_i}\right| \times 100\% \tag{11}$$

$$\delta_{\mathrm{RMSE}} = \sqrt{\frac{1}{n}\sum_{i=1}^{n}(y_i - y_i^{'})^2} \tag{12}$$

Where δ_{MAE} is the mean absolute error (MAE), δ_{MAPE} is the mean absolute percentage error (MAPE), δ_{RMSE} is the root mean square error (RMSE), y_i is the ground truth, $y_i^{'}$ is the K concentration predicted by the different recurrent neural networks, and n is the total number of test samples.

Table 5 shows a comparsion of the evaluation metrics for the RNNs. For the tested biomass fuels and their blends, the K concentration ranges from 2,600 μg/g to 21,495 μg/g. The ratio between the maximum and minimum K concentrations is around 8. The difference in the ground truth of the K concentration between the tested biomass fuels (Table 2) is very large and so is the RMSE of the three prediction models. The MAPE of the three RNN models are all small, indicating good performance of

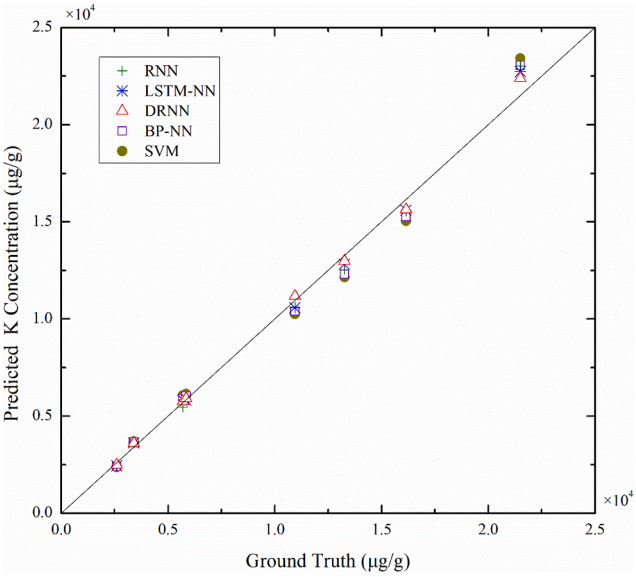

Fig. 14. Predicted K concentration based on the BP-NN, SVM and RNN models.

the models. The training time and computational time for each model are also evaluated, as summarised in Table 5. It is found that the DRNN and LSTM-NN models have a longer computational time than the RNN. It is thought that the architecture of the DRNN model is more complex than those of the RNN and LSTM-NN models, resulting in a longer computational time.

In comparison with the work presented in references [11–16], the online measurement of K concentration is realized through the prediction models instead of experimental analysis of fuels. Other researchers [13,15] established a functional relationship between the spectral intensity of alkali metal, flame temperature, and alkail metal concentration based on experimental data, where the emission characteristics of alkali materials at different combustion temperatures and during different combustion stages were examined. In this paper, however, the models for the prediction of K concentration in a biomass fuel have been established through feature extraction of K spectroscopic signals.

For purpose of a direct comparison with the RNNs, data driven models based on the conventional BP neural network (BP-NN) and

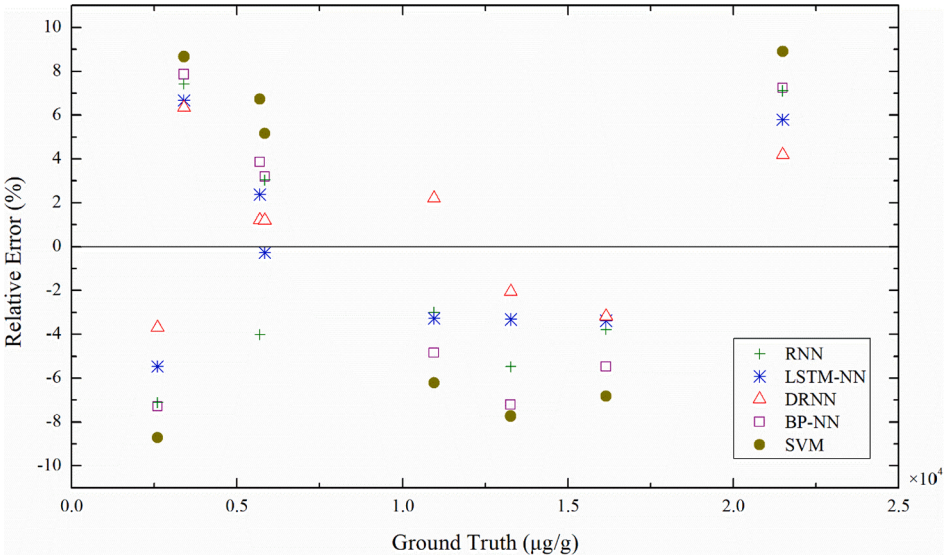

Fig. 15. Relative errors of the RNN models in comparison with the BP-NN and SVM.

support vector machine (SVM) are also established and trained to predict the K concentration of biomass fuels. The BP-NN has a structure of a 7-layer full connection layer with an activation function of Leaky ReLU. In the SVM algorithm the kernel function used is RBF function with kernel parameter of 0.7017 and penalty factor of 0.3536. The comparative results and relative error of all models for the prediction of K concentration are plotted in Fig. 14 and Fig. 15, respectively. The relative error range in the K concentration prediction using the BP-NN and SVM models are (-7.29%, 7.86%) and (-8.71%, 8.91%), respectively. The average errors for the BP-NN and SVM models, i.e. 5.87% and 7.31%, respectively, are consistently greater than those of the three RNNs, which are 5.12%, 3.82% and 3.01%, respectively. It is clear that the RNNs have all outperformed the BP-NN and SVM.

4. Conclusions

The recurrent nerual networks for the dynamic prediction of K concentration in biomass fuels based on the spectroscopic characteristics of flames have been presented. For willow and wheat straw, experimental tests were conducted under different feeder speeds and air flowrates. The results have verified that the emission intensity of alkali depends on alkali concentration in the fuel and that the spectral intensity of K has positive correlation with the fuel flowrate, i.e., the greater the fuel flowrate, the stronger the spectral intensity of K. For the five single biomass fuels and three blends, the spectroscopic distribution of the flame and hence the K concentration are obtained and analysed. The characteristic parameters are analysed, including the flame radiation energy, oscillation frequency, flame temperature and other parameters (e.g., mean, variance, peak-to-peak value, skewness and kurtosis coefficients) of the K spectroscopic signal. The results have demonstrated that these characteristic parameters are good descriptors of the K spectroscopic signal and can thus reflect the combustion behaviours of the biomass fuels. The comparative results in terms of the evaluation metrics have demonstrated that the prediction models, RNN, LSTM-NN and DRNN, have all performed well in predicting the K concentration with the DRNN model slightly outperforms the other two with a relative error within 6.34%. The three RNN models have consistently outperformed the BP-NN and SVM models. In future work the likelihood of slagging in a biomass furnace will be predicted from the K concentration in order to minimise unexpected downtime of the combustion process.

CRediT authorship contribution statement

Xinli Li: Methodology, Validation, Writing - original draft. **Changxing Han:** Software, Validation. **Gang Lu:** Methodology, Writing - review & editing. **Yong Yan:** Funding acquisition, Conceptualization, Supervision, Writing - review & editing.

Declaration of Competing Interest

The authors declare that they have no known competing financial interests or personal relationships that could have appeared to influence the work reported in this paper.

Acknowledgements

The authors wish to acknowledge the National Natural Science Foundation of China (No. 51827808 and No. 61673170) for providing financial support for this research.

References

[1] Huang QL. Development road of green energy. Distributed Energy 2019;4(2):1–7.
[2] Liu D, Liu M, Xiao B, Guo X, Niu D, Qin G, et al. Exploring biomass power generation's development under encouraged policies in China. J Cleaner Prod 2020;258:120786. https://doi.org/10.1016/j.jclepro.2020.120786.
[3] Zhou H, Luo Z, Liu D, Ma W-C. Effect of biomass ashes on sintering characteristics of high/low melting bituminous coal ash. Fuel Process Technol 2019;189:62–73.
[4] Niu Y, Lv Y, Zhang X, Wang D, Li P, Hui S. Effects of water leaching (simulated rainfall) and additives (KOH, KCl, andSiO_2) on the ash fusion characteristics of corn straw. Appl Therm Eng 2019;154:485–92.
[5] Liu YZ, He Y, Wang ZH, et al. Characteristics of alkali species release from a burning coal biomass blend. Appl Energy 2018;215:523–31.
[6] Vassilev SV, Vassileva CG. Methods for characterization of composition of fly ashes from coal-fired power stations: a critical overview. Energy Fuels 2005;19(3):1084–98.
[7] Wang C, Bi H, Lin Q, Jiang X, Jiang C. Co-pyrolysis of sewage sludge and rice husk by TG–FTIR–MS: pyrolysis behavior, kinetics, and condensable/non-condensable gases characteristics. Renewable Energy 2020;160:1048–66.
[8] Hsu L-J, Alwahabi ZT, Nathan GJ, Li Yu, Li ZS, Aldén M. Sodium and potassium released from burning particles of brown coal and pine wood in a laminar premixed methane flame using quantitative Laser-Induced Breakdown Spectroscopy. Appl Spectrosc 2011;65(6):684–91.
[9] Liu Y, He Y, Wang Z, Wan K, Xia J, Liu J, et al. Multi-point LIBS measurement and kinetics modeling of sodium release from a burning Zhundong coal particle. Combustion Flame 2018;189:77–86.
[10] LIM M, Ahmad Zulazalan Shah ZULKIFLI, HASSAN H. Biomass combustion: potassium and sodium flame emission spectra and composition in ash. Journal of the Japan Institute of Energy 2017;96(9):367–71.

[11] Sadeckas M, Striu¯gas N, Andriu¯nas P, Navakas R, Praspaliauskas M, Rabaçal M, et al. Spontaneous emission measurements of selected alkali radicals during the combustion of a single biomass pellet. Energy Fuels 2018;32(10):10132–43.
[12] Paulauskas R, Striūgas N, Sadeckas M, Sommersacher P, Retschitzegger S, Kienzl N. Online determination of potassium and sodium release behaviour during single particle biomass combustion by FES and ICP-MS. Sci Total Environ 2020;746:141162. https://doi.org/10.1016/j.scitotenv.2020.141162.
[13] He Z, Lou C, Fu J, Lim M. Experimental investigation on temporal release of potassium from biomass pellet combustion by flame emission spectroscopy. Fuel 2019;253:1378–84.
[14] He X, Lou C, Qiao Yu, Lim M. In-situ measurement of temperature and alkali metal concentration in municipal solid waste incinerators using flame emission spectroscopy. Waste Manage 2020;102:486–91.
[15] Li K, Yan W, Yu L, Huang X, Chen Y, Zhou H, et al. Simultaneous determination of Na concentration and temperature during zhundong coal combustion using the radiation spectrum. Energy Fuels 2021;35(4):3348–59.
[16] Li K, Yan W, Huang X, Yu L, Chen Y, Lou C. In-situ measurement of temperature and potassium concentration during the combustion of biomass pellets based on the emission spectrum. Fuel 2021;289:119863. https://doi.org/10.1016/j.fuel.2020.119863.
[17] Yang Z-L, Guo X-Q, Chen Z-M, Huang Y-F, Zhang Y-J. RNN-Stega: linguistic steganography based on recurrent neural networks. IEEE Trans Inf Forensics Secur 2019;14(5):1280–95.
[18] Sutskever I, Vinyals O, Le QV. Sequence to sequence learning with neural networks. Neural Information Processing Systems 2014:4104–13112.
[19] Cho K, Merrienboer BV, Gulcehre C, et al. Learning phrase representations using RNN encoder-decoder for statistical machine translation. Computer Science 2014:1724–34.
[20] Elman JL. Finding structure in time. Cognitive science 1990;14(2):179–211.
[21] Hochreiter S, Schmidhuber J. Long short-term memory. Neural Comput 1997;9(8):1735–80.
[22] Hajiabotorabi Z, Kazemi A, Samavati FF, Maalek Ghaini FM. Improving DWT-RNN model via B-spline wavelet multiresolution to forecast a high-frequency time series. Expert Syst Appl 2019;138:112842. https://doi.org/10.1016/j.eswa.2019.112842.
[23] Pham V, Bluche T, Kermorvant C, et al. Dropout improves recurrent neural networks for handwriting recognition. The 14th International Conference on Frontiers in Handwriting Recognition (ICFHR), Greece, Sep. 1-4, 2014: 285-290.
[24] Weerathunga H, Silva A. DRNN-ARIMA approach to short-term trend forecasting in forex market. International Conference on Advances in ICT for Emerging Regions, Sri Lanka, Colombo, Sep. 2018;26–28:287–93.
[25] Huang Y, Yan Y, Lu G, Reed A. On-line flicker measurement of gaseous flames by image processing and spectral analysis. Meas Sci Technol 1999;10(8):726–33.